

# Comparison and analysis of methods for measuring the spin transverse relaxation time of rubidium atomic vapor

Lulu Zhang,<sup>1</sup> Ni Zhao,<sup>1</sup> Yongbiao Yang,<sup>1</sup> Junye Zhao,<sup>1</sup> Jun He,<sup>1,2</sup> and Junmin Wang<sup>1,2, a)</sup>

<sup>1</sup>State Key Laboratory of Quantum Optics and Quantum Optics Decices, Shanxi University, Institute of Opto-Electronics, Taiyuan 030006, China

<sup>2</sup>Collaborative Innovation Center of Extreme Optics, Shanxi University, Taiyuan 030006, China

The spin transverse relaxation time ( $T_2$ ) of atoms is an important indicator in the field of precision measurement. Many methods have been proposed to characterize the  $T_2$  of atoms. In this paper, the  $T_2$  of rubidium (Rb) in the same cell is measured by four measuring methods, namely spin noise spectrum signal fitting, improved free induction decay (FID) signal fitting,  $\omega_m$ -broadening fitting and magnetic resonance broadening fitting. At the same time, the  $T_2$  of five different types of Rb cells were measured and characterized. A comparative analysis visualizes the characteristics of the different measuring methods and the effects of buffer gas pressure filling on  $T_2$  of Rb. By experimental observation, the applicability of the different methods was analyzed, and we concluded that the method of improved FID signal fitting gave the most accurate measurement because of the clean environment in which the measurements were taken. This work can be used to provide another analytical perspective for the selection of the atomic vapor cells and may shed light on the improvement of the sensitivity of atomic magnetometers.

## I. INTRODUCTION

The precise measurement of magnetic fields have very important application potential in basic physics research [1], [2], geophysics [3], clinical medicine [4], and cosmic dark matter measurement [5]. The transverse relaxation time ( $T_2$ ) of atoms is one of the most important indicators to characterize the performance of magnetic field precision measurements. Especially in atomic magnetometers [6], in general, the longer the  $T_2$  of atoms, the higher the magnetic sensitivity of the atomic magnetometer. Since the  $T_2$  of atoms contains a large amount of information, it is very important to accurately and quickly measure the  $T_2$  of atoms to help select the most suitable type of atomic vapor cell.

At present, the traditional free induction decay(FID) method is the most commonly used method for measuring the  $T_2$  of atoms. In 2017, Hui L.'s group [7] proposed the fitting-ratio method and the magnetic resonance broadening method to measure the  $T_2$  of atoms, and compared with the traditional FID method to explore the advantages of the new methods. In 2020, the group proposed a perturbation-free method to measure the  $T_2$  [8] of atoms in nuclear magnetic resonance oscillator. In 2023, Xinye X.'s group [9] measured the  $T_2$  of cesium using three methods.

In addition, the spin noise spectrum signal in spin noise spectroscopy technique also contains a great deal of information. And it is one of the important methods for the measurement of the  $T_2$ . In 2007, Kominis I. K.'s group [10] analyzed the spin noise spectrum properties of atoms in detail from theoretical and experimental perspectives, revealed the relationship between the spin spectrum and the  $T_2$  of atoms.

In this paper, we select spin noise spectrum fitting, improved FID signal fitting,  $\omega_m$ -broadening fitting and magnetic resonance broadening fitting, which are the four methods of

measuring the  $T_2$  of atoms. And five types of rubidium (Rb) vapor cells are selected to measure their  $T_2$ , so as to visually observe the merits of the various methods and the effects of different types of buffer gases on the  $T_2$  of Rb through the comparative analysis of the experimental results.

## II. THEORETICAL ANALYSIS

The relaxation time of an atom is divided into longitudinal relaxation time ( $T_1$ ) and transverse relaxation time. Longitudinal relaxation is the relaxation of the atomic state population to a certain equilibrium value, which is related to the spin of the atom, that is, the lifetime of the atomic state. Transverse relaxation is phase-dependent and refers to the decoherence time of phase.

For alkali metal atomic ensembles, under the action of the static magnetic field  $B_z$  along the z-axis, the components of macroscopic magnetization of atoms in thermal equilibrium are:

$$\begin{aligned} M_z &= M_0, \\ M_x &= M_y = 0. \end{aligned} \quad (1)$$

Here  $M_0$  is a constant value. If a pump light is simultaneously applied along the z-axis to polarize the alkali metal atoms. And an oscillating magnetic field with amplitude  $B_1$ , frequency  $\Omega$  is introduced, whose direction is perpendicular to the static magnetic field  $B_z$ , so that deflect the spin polarization of the alkali metal atoms away from the z-axis. Then the pump light and the oscillating magnetic field are withdrawn, the alkali metal atoms are in a non-equilibrium state, and some relaxation mechanism restores it to a thermal equilibrium state. In a rotating coordinate system, the evolution of the macroscopic magnetization of alkali metal atoms can be given by the Bloch equation, which is described as follows [11]:

<sup>a)</sup>Corresponding author: wwjjmm@sxu.edu.cn; ORCID : 0000-0001-8055-000X

$$\begin{aligned}
\frac{dM'_x(t)}{dt} &= \Delta\omega M'_y(t) - \frac{M'_x(t)}{T_2}, \\
\frac{dM'_y(t)}{dt} &= \gamma B_1 M_z(t) - \Delta\omega M'_x(t) - \frac{dM'_y(t)}{T_2}, \\
\frac{M_z(t)}{dt} &= -\gamma B_1 M'_y(t) + \frac{M_0 - M_z(t)}{T_1}.
\end{aligned} \tag{2}$$

Here  $\Delta\omega$  is the mismatch between the Larmor frequency and the oscillating magnetic field frequency,  $\gamma$  is the ground-state gyromagnetic ratio. In this process, the macroscopic magnetization of alkali metal atoms is decomposed into a component  $M_z$  parallel to the static magnetic field and components  $M_x, M_y$  perpendicular to the static magnetic field. The characteristic time from  $M_z$  to  $M_0$  is referred to as the longitudinal relaxation time. The characteristic time for  $M_x$  and  $M_y$  to gradually return to 0 is called the transverse relaxation time, in which the spin precession phase of the alkali metal atoms is redistributed until it is disordered.

### A. Spin noise spectrum fitting

Spin noise is the random distribution of atomic electron spins in quasi-thermodynamic equilibrium. The spin noise spectrum is an optical technique that can be measured by nuclear magnetic resonance and magnetic force microscopy, but the most sensitive and widely used detection technique is Faraday rotation, which maps atomic spin noise on the polarization plane of a non-resonant detection light. We have also experimentally measured and explored the atomic spin noise spectrum in previous articles [12], [13], and have a certain understanding of its principle and parameter optimization.

The other is the Voigt configuration, the light beam is perpendicular to magnetic field, the random fluctuation of magnetization precess around the direction of the static magnetic field, and this fluctuation on the spectrum manifests as Lorentzian-linear peak. The full width at half maximum(FWHM) of the peak is inversely correlated with the  $T_2$  [15]. This is also the experimental setup used in our apparatus to measure the  $T_2$ .

### B. The FID signal fitting

In this method, an all-optical line Bell-Bloom magnetometer [16] modulated with pump light and a magnetometer driven by radio frequency(RF) magnetic field [17] are the two most commonly used experiment setups. In Bell-Bloom magnetometer, the direction of the static magnetic field is perpendicular to the pump light, which is modulated in frequency or amplitude. In RF magnetometer, the direction of the pump light is parallel to the static magnetic field, and an oscillating magnetic field with the Larmor frequency is used for  $\pi/2$  pulse times. These two approaches cause the macroscopic magnetization of the atomic ensemble to be acted upon in a plane perpendicular to the static magnetic field, and the precession

is exponentially attenuated around the static magnetic field at the Larmor frequency. This Larmor precession is mapped to the rotation of the polarization plane of the probe light, and the FID signal is subsequently detected with a differential detector. The  $T_2$  of the atom can be obtained [18], [19] simply by fitting the envelope of the FID signal:

$$S_{FID} = A_{FID} \exp(-t/T_2) \tag{3}$$

Here, we use an atomic magnetometer driven by a RF magnetic field, and the traditional method of obtaining the FID signal is improved and optimized, that is, the action time of the pump light, the detection light and the RF magnetic field in the time domain is controlled by the timing sequence, so as to avoid the signal being affected by the pump light and the additional magnetic field during the detection[20].

### C. $\omega_m$ -broadening fitting

In this method, a modulated magnetic field with frequency  $\omega_m$  is applied in the direction of the static magnetic field  $B_z$ , and if there are magnetic fields  $B_x$  and  $B_y$  in the x and y directions that are much smaller than  $B_z$ , then the expression of the in-phase and quadrature phase signals after LIA demodulation is [9]:

$$\begin{aligned}
S_{IS} &\propto \frac{B_y - B_x(\gamma B_z + n\omega_m)T_2}{1 + T_2^2(\gamma B_z + n\omega_m)^2}, \\
S_{QS} &\propto \frac{B_x - B_y(\gamma B_z + n\omega_m)T_2}{1 + T_2^2(\gamma B_z + n\omega_m)^2}.
\end{aligned} \tag{4}$$

where n is the ratio of the Larmor frequency  $\omega_0$  to the modulation frequency  $\omega_m$ , i.e.,  $n = \omega_0 / \omega_m$ . When  $B_x \neq 0$ ,  $B_y = 0$ , the above equation can be written as:

$$\begin{aligned}
S_{IS} &\propto \frac{B_x(\gamma B_z + n\omega_m)T_2}{1 + T_2^2(\gamma B_z + n\omega_m)^2}, \\
S_{QS} &\propto \frac{B_x}{1 + T_2^2(\gamma B_z + n\omega_m)^2}.
\end{aligned} \tag{5}$$

Similarly we can also find the in-phase and quadrature phase signals of the LIA demodulation in case  $B_x = 0$ ,  $B_y \neq 0$ . From the above equation, it can be obtained:  $\Gamma_{QS} = \Gamma_{IS} = 2/nT_2$ .

### D. Magnetic resonance broadening fitting

In this method, an RF magnetic field of magnitude  $B_1$ , frequency  $\Omega$  is applied perpendicular to the direction of the static magnetic field. In a rotating coordinate system, the steady-state solution of the magnetization  $M$  is [21]:

$$\begin{aligned}
M_x &= \frac{M_0 \gamma B_1 \Delta \omega}{(1/T_2)^2 + (\Delta \omega)^2 + (T_1/T_2)(\gamma B_1)^2}, \\
M_y &= \frac{M_0 \gamma B_1 (1/T_2)}{(1/T_2)^2 + (\Delta \omega)^2 + (T_1/T_2)(\gamma B_1)^2}, \\
M_z &= \frac{M_0 [(\Delta \omega)^2 + (1/T_2)^2]}{(1/T_2)^2 + (\Delta \omega)^2 + (T_1/T_2)(\gamma B_1)^2}.
\end{aligned} \tag{6}$$

$\Delta \omega = \omega_L - \Omega$  is the mismatch between the Larmor frequency and the oscillating magnetic field frequency. Scanning the static magnetic field  $B_0$ , the relationship between the FWHM and  $B_1$  after LIA is [7] :

$$\Gamma = 2\sqrt{(1/T_2)^2 + T_1/T_2}(\gamma B_1)^2 \tag{7}$$

And  $\Gamma = 2/T_2$  when the RF magnetic field strength is small enough to be negligible.

### III. EXPERIMENTAL SETUP

The experimental setup is shown in Fig. 1, in which a cubic  $^{87}\text{Rb}$  vapor cell, contains 100 Torr  $N_2$ , with an length of 15 mm was used for the experiment. The AC-driven non-magnetic heating films and feedback loop act as a heating system to control the temperature of the atomic vapor cell at 75 °C. The cell is housed within four layers of  $\mu$ -metal magnetic shielding to shield the ambient magnetic field, and a three-axis Helmholtz coil is placed inside to generate a magnetic field, where the direction of the static magnetic field is along the z-axis.

The magnetometer configuration is shown in Fig. 1(a), The pump light from the 795 nm external cavity semiconductor laser (ECDL) passes through the acousto-optic modulator (AOM), beam expander, and quarter-wave plate into a circularly polarized pumped light with a beam diameter of  $\sim 10$  mm, and then enters the rubidium atomic vapor cell along the z-axis. In the experiment, depending on the type of atomic vapor cell, the frequency of the pump light is locked at the  $^{87}\text{Rb}$  D1 line  $F=2-F'=1$  transition line or the  $^{85}\text{Rb}$  D1 line  $F=3-F'=2$  transition line. The pump light intensity entering the cell is  $12.74 \text{ mW}/\text{cm}^2$ . The probe light from the 780 nm distributed Bragg reflective (DBR) laser also passes through the AOM and the polarizer to become linearly polarized light with a beam diameter of  $\sim 2$  mm. The frequency of the probe light is 18 GHz blue detuned from the D2 transition line of Rb, and the light intensity entering the cell is  $3.18 \text{ mW}/\text{cm}^2$ . After traversing the cell along the x-axis, the probe light enters a balanced polarimeter where the optical signal is converted into an electrical signal and feed into the lock-in amplifier(LIA).

For the spin noise spectroscopy configuration, as shown in Fig. 1(b), the direction of the static magnetic field is also along the z-axis. Only a 780 nm linearly polarized probe light is used to traversing the vapor cell along the x-axis. The rotation of the probe light polarization received by the balanced polarimeter, subsequently into the fast Fourier transform (FFT)

to convert the time-domain signal into a frequency-domain signal.

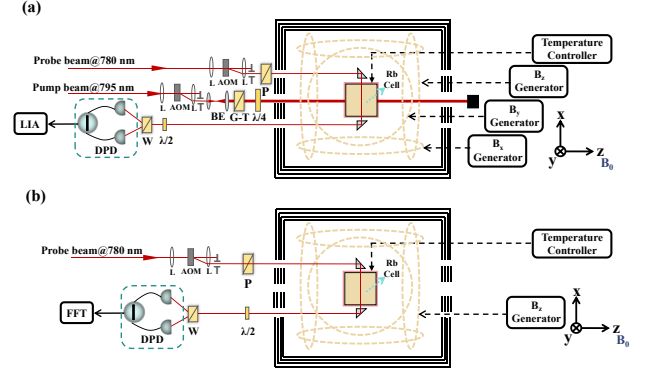


FIG. 1. (a) Rubidium atomic magnetometer scheme. (b) Spin noise spectroscopy scheme. AOM: acoustic-optical modulator; BE: beam expander;  $\lambda/4$ : quarter-wave plate;  $\lambda/2$ : half-wave plate; G-T: Glen Taylor Prism; L: lens P: polarizer; W: Wollaston prism; DPD: Differential photodetector; LIA: Lock-in Amplifier; FFT: Fast Fourier Transform.

### IV. RESULTS AND ANALYSIS

#### A. Typical four measuring methods results and analysis

In the experimental measurements, we set the static magnetic field  $B_0 = 6.32 \mu\text{T}$  for a cubic  $^{87}\text{Rb}$  vapor cell, with a length of  $15 \text{ mm} \times 15 \text{ mm} \times 15 \text{ mm}$ , filled with 100 Torr  $N_2$ . A typical spin noise spectrum signal, measured by the spin noise spectrum method, is shown in Fig. 2. We set the average sample number to 1000 times, optimized the parameters, and obtained a full width at half maximum(FWHM) of 1.5 kHz by lorentz fitting.

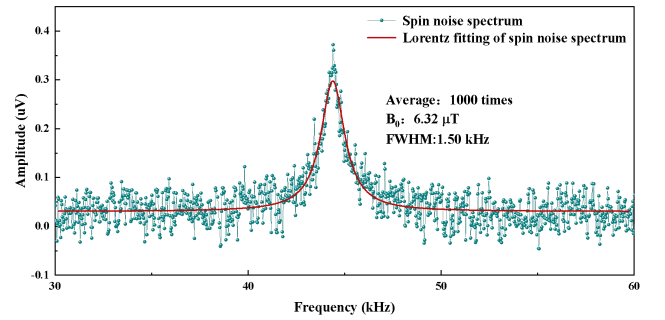


FIG. 2. Spin noise spectrum signal. The red curve is the lorentz fitting, with a typical HWHM of 1.50 kHz. Other parameters: the frequency of the probe beam power is blue detuning 10 GHz relative to the D2 line of the  $^{87}\text{Rb}$ . The spin noise spectrum is averaged 1000 times and  $B_0$  is  $6.32 \mu\text{T}$ .

In the FID signal fitting method, we design a timing sequence control system to separate the pump light, RF mag-

netic field, and probe light from the time domain, so as to avoid the influence of crosstalk between the three on the free-induced attenuation signal[22]. Here we set the typical timing sequence as 10 ms for the pump light time, 3 mA for the current to apply the RF magnetic field strength, the corresponding  $\pi/2$  pulse time of 0.2 ms, and the detection time of 29.8 ms. Typical experimental results are shown in Fig. 3, and the  $T_2$  of Rb is 3.7 ms by fitting Eq.(3).

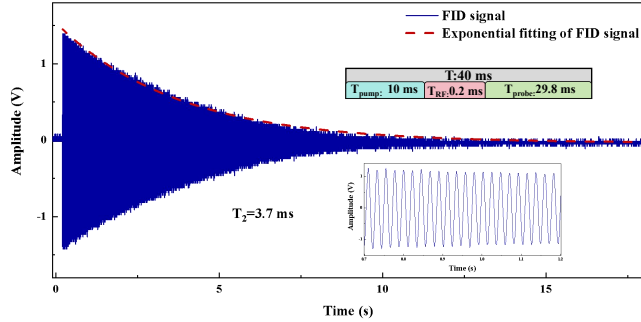


FIG. 3. The FID signal. The red dotted line is the exponential fitting. Inset: timing sequence control system (top) and several FID precession cycle (bottom).

In  $\omega_m$  - Broadening fitting method, We set the frequency  $\omega_m$  of the modulation field to half the Lamor frequency  $\omega_L$ , i.e.  $n=2$ , and sweep the frequency near the modulated frequency. Set  $B_x = 0.41 \mu\text{T}$ ,  $B_y = 0 \mu\text{T}$  or  $B_x = 0 \mu\text{T}$ ,  $B_y = 0.41 \mu\text{T}$ . A typical in-phase and quadrature signals obtained by LIA is shown in Fig. 4, where  $\omega_m$  is also the reference frequency of LIA, the extracted  $T_2$  of Rb is 3.9 ms.

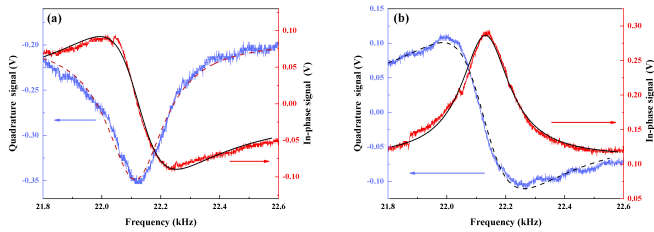


FIG. 4. (a) The demodulated in-phase and quadrature signals when  $B_x = 0.41 \mu\text{T}$ ,  $B_y = 0 \mu\text{T}$ . (b) The demodulated in-phase and quadrature signals when  $B_x = 0 \mu\text{T}$ ,  $B_y = 0.41 \mu\text{T}$ .

In magnetic resonance broadening fitting experiments, We apply an RF magnetic field with a frequency equal to the Lamor frequency on the y-axis, and the reference signal frequency demodulated by the LIA is also set to the Lamor frequency, and the static magnetic field applied on the z-axis is scanned, and the in-phase and quadrature signals are shown in Figure 5(a). The FWHM is obtained by Lorentz fitting of the demodulated signal. With the change of RF magnetic field strength, the variation of FWHM with RF magnetic field strength is shown in Fig. 5(b). According to Eq. (6), the  $T_2$  of Rb is 3.0 ms

## B. Comparison and analysis of different types of rubidium vapor cells

We also selected five types of rB vapor cells, the parameters of which are shown in Table 1, and used the above four methods to measure the  $T_2$  of Rb in different Rb vapor cells. Typical results are shown in Fig. 6(a). The figure shows that the  $20 \text{ mm} \times 20 \text{ mm} \times 20 \text{ mm}$  purified  $^{87}\text{Rb}$  vapor cell filled with 100 Torr  $N_2$  have the best suppression of atomic spin decoherence.

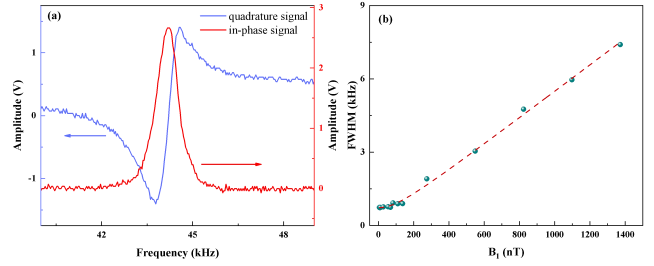


FIG. 5. (a) The in-phase and quadrature signals while  $B_1 = 69 \text{ nT}$ . (b) Dependence between FWHM and RF magnetic field strength.

It is also evident from Fig. 6 (a) that the  $T_2$  obtained by the spin noise spectrum method is significantly smaller than that of the other three methods. We compare the FWHM obtained by FFT of the FID signal with the FWHM of the spin noise spectrum, as shown in Fig. 6(b). The FWHM of the spin noise spectrum signal is significantly wider than the FWHM of the FID signal after FFT. The main reasons are as follows. Firstly, the spin noise spectrum measures atomic spins' fluctuations under unpolarization, which yields a relatively small signal amplitude and a poor signal-to-noise ratio. At the same time, the power broadening and the inhomogeneity of the probe light in the Rb cell can also have a negative effect. Secondly, due to the influence of the transit time broadening and the measurement time. And they interact with each other. The longer the measurement time, the more times the atoms cross the probe beam, and the wider the line broadening caused by the crossing time. Furthermore, the inhomogeneity of the static magnetic field also affects the FWHM, further influence the  $T_2$  of Rb.

TABLE I. Specification parameters of the five rubidium vapor cells

Cell number	Cell size (mm)	Other gas filled into cell
NO.1	15×15×15	$^{87}\text{Rb}$ +100 Torr $N_2$
NO.2	20×20×20	$^{87}\text{Rb}$ + $^{85}\text{Rb}$ +100 Torr $N_2$ +20 Torr He
NO.3	20×20×20	$^{87}\text{Rb}$ +100 Torr $N_2$
NO.4	20×20×20	$^{87}\text{Rb}$ + $^{85}\text{Rb}$ +100 Torr $N_2$
NO.5	20×20×20	$^{87}\text{Rb}$ + $^{85}\text{Rb}$ +600 Torr $N_2$ +50 Torr He

In addition to the spin noise spectrum method, the other three methods also have differences in measurement results due to the different magnetic fields at the time of measure-

ment, but the three methods can be used for different types of magnetometers. Since only static magnetic field exists in the measurement process and the time-sequence control system avoids the negative effect of pump light in the measurement, the whole measurement process is cleaner in terms of environmental factors, and relatively more accurate  $T_2$  of Rb are obtained from the measurement.

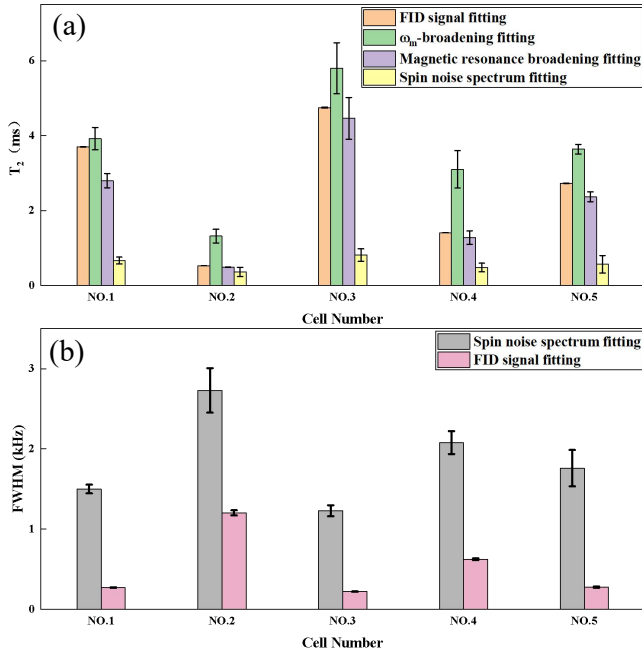


FIG. 6. (a) The  $T_2$  of Rb measured by FID signal fitting,  $\omega_m$  - broadening fitting, magnetic resonance broadening fitting and Spin noise spectrum fitting in different Rb vapor cells. (b) The FWHM of FID signal fitting and Spin noise spectrum fitting in different Rb vapor cells.

In our study, we filled Rb cells with buffer gas to suppress the negative effects of spin-destructive collisional relaxation on  $T_2$  of Rb. Besides, spin-exchange collision relaxation is also one of the dominant relaxation mechanisms. Based on the FID signal fitting method, we experimentally measured the dependence between different temperatures and the  $T_2$  of Rb. The same  $15\text{ mm} \times 15\text{ mm} \times 15\text{ mm}$ , square Rb cell filled with 100 Torr  $N_2$  were used, and typical results are shown in Fig. 7. The  $T_2$  of Rb is positively correlated with the atomic number density at low temperatures. As the atomic number density further increases, the  $T_2$  of Rb gradually decreases due to the dominant mechanism of spin-exchange collisional relaxation.

## V. CONCLUSIONS

In this paper, we select four methods to measure the  $T_2$  of Rb based on the Rb vapor cell filled with different types and pressures buffer gas. Among the mechanisms affecting the  $T_2$  of Rb, spin destruction collision and spin exchange collision are the two dominant relaxation mechanisms. Here we demonstrate the suppression of spin-destructive collisions

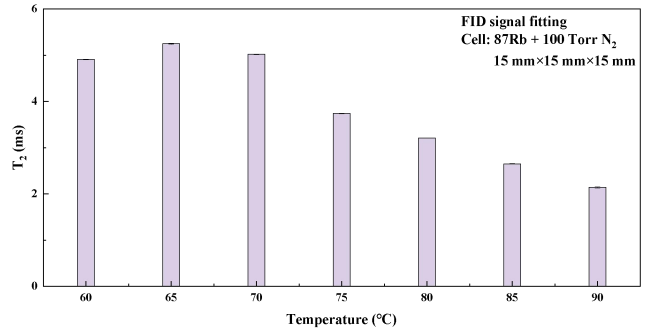


FIG. 7. Dependence between different temperatures and the  $T_2$  of Rb. Cell parameters:  $15\text{ mm} \times 15\text{ mm} \times 15\text{ mm}$ ,  $^{87}\text{Rb} + 100\text{ Torr } N_2$

by filling buffer gases of different types and pressures. The effect of spin-exchange collisions on  $T_2$  was demonstrated by varying the atomic number density. Suppression of spin-exchange collisions can be achieved by optical narrowing effects[23],[24] or by heating the cell to extremely high temperatures to a spin-exchange relaxation-free state[25],[26].

Among these four methods, the  $T_2$  of Rb obtained by the spin noise spectrum fitting method is less than the actual value due to the limitation of the measurement technology, and a high-resolution spin noise spectrometer is required for experimental acquisition. But this method provides a roundabout method for comparing the  $T_2$  of atoms in different types of atomic vapor cell. The experimental setup for the magnetic resonance broadening fitting method is relatively simple. It is easier to implement experimentally, and even the  $T_2$  of atoms can be measured only by measuring the pump light [7]. The  $\omega_m$  - broadening fitting method allows real-time monitoring of the drift of the static magnetic field, which can be compensated by a servo-loop system. Although the experimental setup for the improved FID signal fitting method is relatively complex, it ensures that the negative effects of the RF magnetic field and pump light are not introduced during the measurement by applying a timing sequence control system. And the  $T_2$  of atoms measured by this method is relatively accurate.

These four methods can be used in different measuring environments. The  $T_2$  of atoms obtained by different measuring methods are somewhat different, mainly because the magnetic field environment is different during the measurement. But all of them intuitively show the relationship between the buffer gases of different pressures and the  $T_2$  of atoms. This provides a variety of feasible methods for future precision measurement fields, such as the improvement of the sensitivity of atomic magnetometers and the selection of atomic vapor cells. At the same time, by comparing the  $T_2$  of Rb obtained by five different types of Rb vapor cells under the same conditions, we can obtain an optimal type of atomic vapor cell. This study has important application reference value in the fields of the fabrication of atomic vapor cell, the types of buffer gases to be filled and the selection of pressure.

## FUNDING

This work was supported by the National Natural Science Foundation of China (Grant Nos. 11974226) and the Shanxi Provincial Graduate Education Innovation Project (Grant No.2022Y022).

## REFERENCES

- <sup>1</sup> S.-K. Lee, K. L. Sauer, S. J. Seltzer, O. Alem, M. V. Romalis, “Subfemtotesla radio-frequency atomic magnetometer for detection of nuclear quadrupole resonance,” *Appl. Phys. Lett.*, vol. 89, no. 21, Nov. 2006, Art. no. 214106.
- <sup>2</sup> J. M. Brown, S. J. Smullin, T. W. Kornack, M. V. Romalis, “New limit on Lorentz- and CPT-violating neutron spin interactions,” *Phys. Rev. Lett.*, vol. 105, no. 15, Oct. 2010, Art. no. 151604.
- <sup>3</sup> M. N. Nabighian, V. J. S. Grauch, R. O. Hansen, T. R. LaFehr, Y. Li, J. W. Peirce, J. D. Phillips, M. E. Ruder, “The historical development of the magnetic method in exploration,” *Geophysics*, vol. 70, no. 6, pp. 33ND–61ND, Dec. 2005.
- <sup>4</sup> R. Zhang, W. Xiao, Y. Ding, Y. Feng, X. Peng, L. Shen, C. Sun, T. Wu, Y. Yang, Z. Zheng, X. Zhang, J. Chen, H. Guo, “Recording brain activities in unshielded Earth’s field with optically pumped atomic magnetometers,” *Adv. Sci.*, vol. 6, no. 24, Jun. 2020, Art. no. eaba8792.
- <sup>5</sup> M. Jiang, H. Su, A. Garcon, X. Peng, D. Budker, “Search for axion-like dark matter with spin-based amplifiers,” *Nat. Phys.*, vol. 17, no. 12, pp. 1402–1407, Dec. 2021.
- <sup>6</sup> H. Crepaz, L. Y. Ley, R. Dumke, “Cavity enhanced atomic magnetometry,” *Sci. Rep.*, vol. 5, no. 1, Oct. 2015, Art. no. 15448.
- <sup>7</sup> P. Jiang, Z. Wang, H. Luo, “Techniques for measuring transverse relaxation time of xenon atoms in nuclear-magnetic-resonance gyroscopes and pump-light influence mechanism,” *Optik*, vol. 138, pp. 341–348, Jun. 2017.
- <sup>8</sup> C. Chen, Q. Jiang, Z. Wang, Y. Zhang, H. Luo, K. Yang, “A non-interference method for measurement of transverse relaxation time of the alkali metal magnetometer in nuclear magnetic resonance oscillator,” *AIP Adv.*, vol. 10, no. 6, Jun. 2020, Art. no. 065303.
- <sup>9</sup> M. Wei, W. Yu, M. Zhou, W. Huang, Y. Liu, X. Xu, “Three techniques for measuring the transverse relaxation time of cesium atoms,” *AIP Adv.*, vol. 13, no. 3, Mar. 2023, Art. no. 035327.
- <sup>10</sup> G. E. Katsoprinakis, A. T. Dellis, I. K. Kominis, “Measurement of transverse spin-relaxation rates in a rubidium vapor by use of spin-noise spectroscopy,” *Phys. Rev. Appl.*, vol. 75, no. 4, Apr. 2007, Art. no. 042502.
- <sup>11</sup> F. Bloch, “Nuclear Induction,” *Phys. Rev.*, vol. 70, no. 7, pp. 460–474, Oct. 1946.
- <sup>12</sup> Y. Yang, L. Bai, L. Zhang, J. He, X. Wen, J. Wang, “Experimental investigation of spin noise spectroscopy of rubidium atomic ensemble,” *Acta Phys. Sin.*, vol. 69, no. 23, Dec. 2022, Art. no. 233201.
- <sup>13</sup> L. Bai, L. Zhang, Y. Yang, R. Chang, Y. Qin, J. He, X. Wen, J. Wang, “Enhancement of spin noise spectroscopy of rubidium atomic ensemble by using the polarization squeezed light,” *Opt. Express*, vol. 30, no. 2, pp. 1925–1936, Jan. 1946.
- <sup>14</sup> V. S. Zapasskii, “Spin-noise spectroscopy: from proof of principle to applications,” *Adv. Opt. Photonics*, vol. 5, no. 2, pp. 131–168, Jun. 2013.
- <sup>15</sup> J. Hübner, F. Berski, R. Dabashi, M. Oestreich, “The rise of spin noise spectroscopy in semiconductors: From acoustic to GHz frequencies,” *Phys. Status Solidi B* vol. 251, no. 9, pp. 1824–1838, Sep. 2014.
- <sup>16</sup> D. Hunter, S. Piccolomo, J. D. Pritchard, N. L. Brockie, T. E. Dyer, E. Riis, “Free-Induction-Decay Magnetometer Based on a Microfabricated Cs Vapor Cell,” *Phys. Rev. Appl.*, vol. 10, no. 1, Jul. 2018, Art. no. 014002.
- <sup>17</sup> S. Li, J. Liu, M. Jin, K. T. Akiti, P. Dai, Z. Xu, Eric-Theophilus Nwodom T., “A kilohertz bandwidth and sensitive scalar atomic magnetometer using an optical multipass cell,” *Measurement*, vol. 190, Feb. 2022, Art. no. 110704.
- <sup>18</sup> H. Dong, H. Liu, J. Ge, Z. Yuan, Z. Zhao, “A High-Precision Frequency Measurement Algorithm for FID Signal of Proton Magnetometer,” *IEEE Trans. Instrum. Meas.* vol. 65, no. 4, pp. 898–904, Apr. 2016.
- <sup>19</sup> H. Li, Mi. Jiang, Z. Zhu, W. Xu, M. Xu, X. Peng, “Calibration of magnetic field measurement capability of rubidium-xenon vapor cell atomic magnetometer,” *Acta Phys. Sin.*, vol. 68, no. 16, Aug. 2019, Art. no. 160701.
- <sup>20</sup> L. Zhang, Y. Yang, N. Zhao, J. He, J. Wang, “A Multi-Pass Optically Pumped Rubidium Atomic Magnetometer with Free Induction Decay,” *Sensors*, vol. 22, no. 19, Oct. 2022, Art. no. 7598.
- <sup>21</sup> D. Budker, D. Jackson Kimball, “Optical Magnetometry,” in *Atomic physics, molecular physics and chemical physics*, Cambridge: Cambridge University Press, 2013, pp. 60–63.
- <sup>22</sup> W. Zheng, X. Bi, G. Zhang, S. Su, J. Li, Q. Lin, “Experimental Demonstration of Light Narrowing Effect

Based on Free Atomic Spin Precession,” *Chin. J. Lasers*, vol. 47, no. 3, Mar. 2020, Art. no. 0304001.

<sup>23</sup> S. Appelt, A. Ben-Amar Baranga, A. R. Young, W. Happer, “Light narrowing of rubidium magnetic-resonance lines in high-pressure optical-pumping cells,” *Phys. Rev. A*, vol. 59, no. 3, Mar. 1999, pp. 2078–2084.

<sup>24</sup> Y.-Y. Jau, A. B. Post, N. N. Kuzma, A. M. Braun, M.V. Romalis, W. Happer, “Intense, Narrow Atomic-Clock

Resonances,” *Phys. Rev. Lett.*, vol. 92, no. 11, Mar. 2004, Mar. no. 110801.

<sup>25</sup> I.K.Kominis, T.W.Kornack, J.C.Allred, M.V.Romalis, “A subfemtotesla multichannel atomic magnetometer,” *Nature*, vol. 422, Apr. 2003, pp. 596-599.

<sup>26</sup> J. Li, W. Quan, B. Zhou, Z. Wang, W. Lu, Z. Hu, G. Liu, J. Fang, “A Review of SERF atomic magnetometer: recent advances and applications,” *IEEE Sensors Journal*, vol. 18, no. 20, Oct. 2018, pp. 8198-8207.